NASA TECHNICAL MEMORANDUM

NASA TM X-1134

PRESSURE-RISE CHARACTERISTICS FOR A LIQUID-HYDROGEN DEWAR FOR HOMOGENEOUS, NORMAL-GRAVITY QUIESCENT, AND ZERO-GRAVITY TESTS

by Kaleel L. Abdalla, Thomas C. Frysinger, and Charles R. Andracchio

Lewis Research Center
Cleveland, Ohio

NATIONAL AERONAUTICS AND SPACE ADMINISTRATION • WASHINGTON, D. C. • SEPTEMBER 1965

[redacted]

NASA TM X-1134

PRESSURE-RISE CHARACTERISTICS FOR A LIQUID-HYDROGEN DEWAR FOR HOMOGENEOUS, NORMAL-GRAVITY QUIESCENT, AND ZERO-GRAVITY TESTS

By Kaleel L. Abdalla, Thomas C. Frysinger, and Charles R. Andracchio

Lewis Research Center
Cleveland, Ohio

[redacted]
GROUP 4
Downgraded at 3-year intervals;
declassified after 12 years

[redacted]
CLASSIFIED DOCUMENT–TITLE UNCLASSIFIED
This material contains information affecting the national defense of the United States within the meaning of the espionage laws, Title 18, U.S.C., Secs. 793 and 794, the transmission or revelation of which in any manner to an unauthorized person is prohibited by law.

NOTICE
This document should not be returned after it has satisfied your requirements. It may be disposed of in accordance with your local security regulations or the appropriate provisions of the Industrial Security Manual for Safe-Guarding Classified Information.

NATIONAL AERONAUTICS AND SPACE ADMINISTRATION

[redacted]

PRESSURE-RISE CHARACTERISTICS FOR A LIQUID-HYDROGEN DEWAR FOR HOMOGENEOUS, NORMAL-GRAVITY QUIESCENT, AND ZERO-GRAVITY TESTS (U)

by Kaleel L. Abdalla, Thomas C. Frysinger, and Charles R. Andracchio

Lewis Research Center

SUMMARY

The pressure-rise characteristics for a liquid-hydrogen Dewar were obtained by utilizing a scientific passenger pod on an Atlas intercontinental ballistic missile during a 21-minute gravity free flight. Results were compared with those from homogeneous and normal-gravity quiescent tests. Residual pod rotation created an undesirable acceleration field on the Dewar of approximately 10^{-3} g throughout the weightless flight time. Temperature instrumentation indicated wall drying during this period. The resultant pressure-rise characteristics were similar to those for the normal-gravity test.

INTRODUCTION

Since the inception of utilizing high-energy propellants, such as liquid hydrogen, to power vehicles for space missions, the study of the heat-transfer mechanism and, in particular, the liquid configuration and pressure-rise characteristics during weightlessness, has become essential to nearly all participating space vehicles. During this time the NASA Lewis Research Center has been conducting an extensive program to determine the static and dynamic behavior of liquids in a weightless environment and a parallel program to investigate the pressure-rise characteristics of basic tank configurations in both normal-gravity and zero-gravity environments. A summary of the overall program to date along with the contributions of others is presented in reference 1. Hydrodynamic and configuration studies of basic wetting and nonwetting liquids in the absence of heat

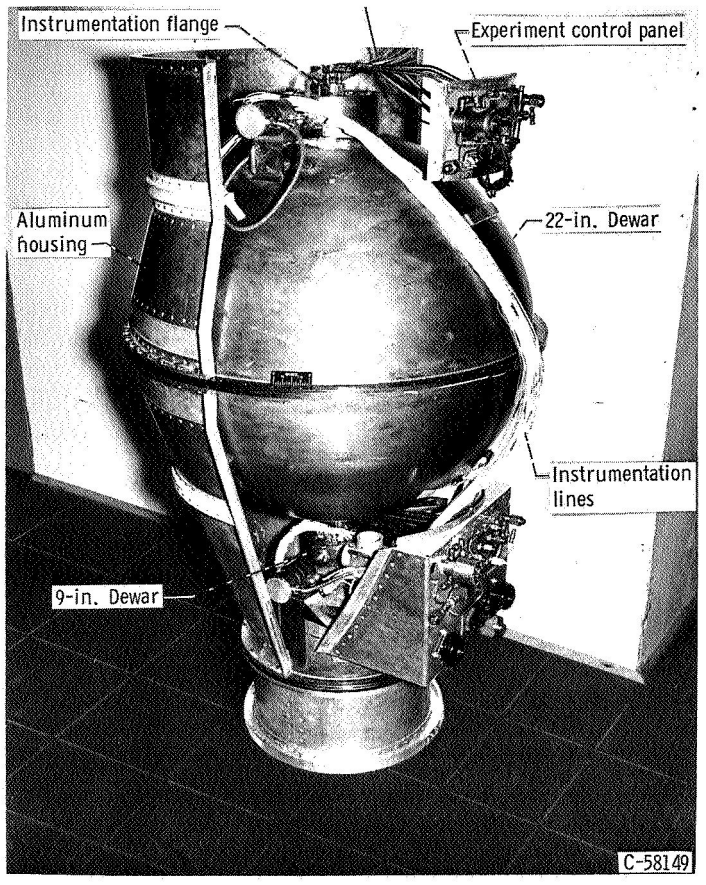

Figure 1. - Typical experiment assembly in housing.

transfer have been made (refs. 2 to 12) that define the liquid-vapor configuration and the predominant parameters that predict the equilibrium zero-gravity configuration.

In conjunction with the basic liquid behavior studies, a series of zero-gravity tests aboard Aerobee sounding rockets was conducted. These experiments consisted of 9-inch-diameter spherical Dewars, partially filled with liquid hydrogen and subjected to a controlled, radiation-heated environment. Based on the work of references 2 to 12 and on boiling heat-transfer studies (refs. 13 to 18), zero-gravity and reference normal-gravity data were obtained for varying conditions including heat flux, flux symmetry, liquid configuration, and liquid depth for a time period of the order of 4 to 7 minutes. These data are reported in references 19 to 26. For most of these experiments the zero-gravity time available was sufficient to establish steady-state or limiting conditions. However, for those experiments at low heat flux, approximately 25 Btu per hour per square foot (ref. 25), the data indicate that more time was necessary to reach quasi-equilibrium or limiting conditions so that time extrapolated predictions could be made.

An experiment package, therefore, was designed to be carried piggyback on board an Atlas intercontinental ballistic missile in order to provide a weightless environment of the order of 1/2 hour. The experiment was similar to that of reference 25 and was placed along with other experimentation in a scientific passenger pod.

The experiment package was thoroughly flight qualified at the Lewis Research Center. Prior to the flight a series of normal-gravity tests was obtained. Then the experiment, plus associated equipment and hardware, was taken to the Atlantic Missile Range where it was launched on February 25, 1964. Final conditions for the experiment were a liquid filling of 36 percent and a heat flux of approximately 25 Btu per hour per square foot.

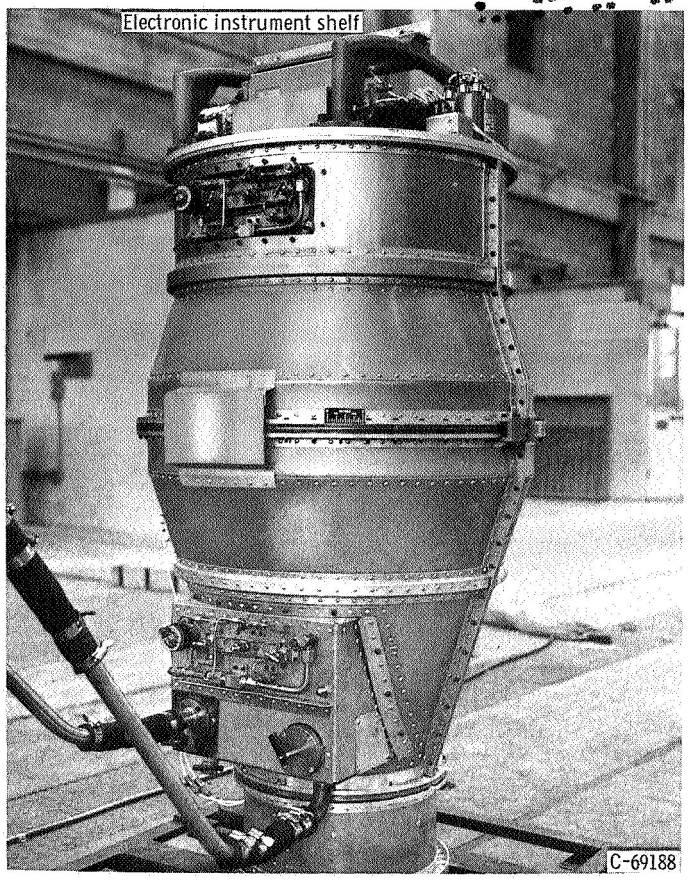

Figure 2. - Flight experiment with electronic instrument shelf.

APPARATUS

General Description

The flight experiment consisted of a spherical vacuum-jacketed Dewar installed in an aluminum housing along with a similar but larger Dewar (fig. 1). An electronic instrument shelf was bolted on the top of the experiment as shown in figure 2. This assembly, along with associated hardware, was mounted inside a scientific passenger pod as shown in figure 3. Details of the pod are given in reference 27, in addition to specifications of the battery power supply, programer, and telemetry system incorporated in the module. The complete pod with ejection mechanism and fairing was designed to fit piggyback aboard the Atlas intercontinental ballistic missile as shown in figure 4. The flight experiment without the passenger pod was used for the normal-gravity quiescent and the shake tests. For these tests an external power source and telemetry system were employed.

Experiment Description

The experiment consisted of a 9-inch-diameter spherical, vacuum-jacketed Dewar (fig. 5). The liquid-hydrogen container was a 0.030-inch-thick wall, stainless-steel sphere, whose outer surface was polished to a maximum 4-microinch mirror finish. The outer sphere was a stainless-steel vacuum jacket, flanged for assembly and instrumentation. The inner surface of this sphere was gold plated and had a maximum 4-microinch mirror finish. The intermediate sphere was similarly polished but had a gold-plated outer surface. This intermediate shell contained heating elements wound around the outer surface to which electrical power was controlled in order to provide a calibrated radiant heat flux.

The Dewar assembly, whose parts are shown in figure 6, was so designed and

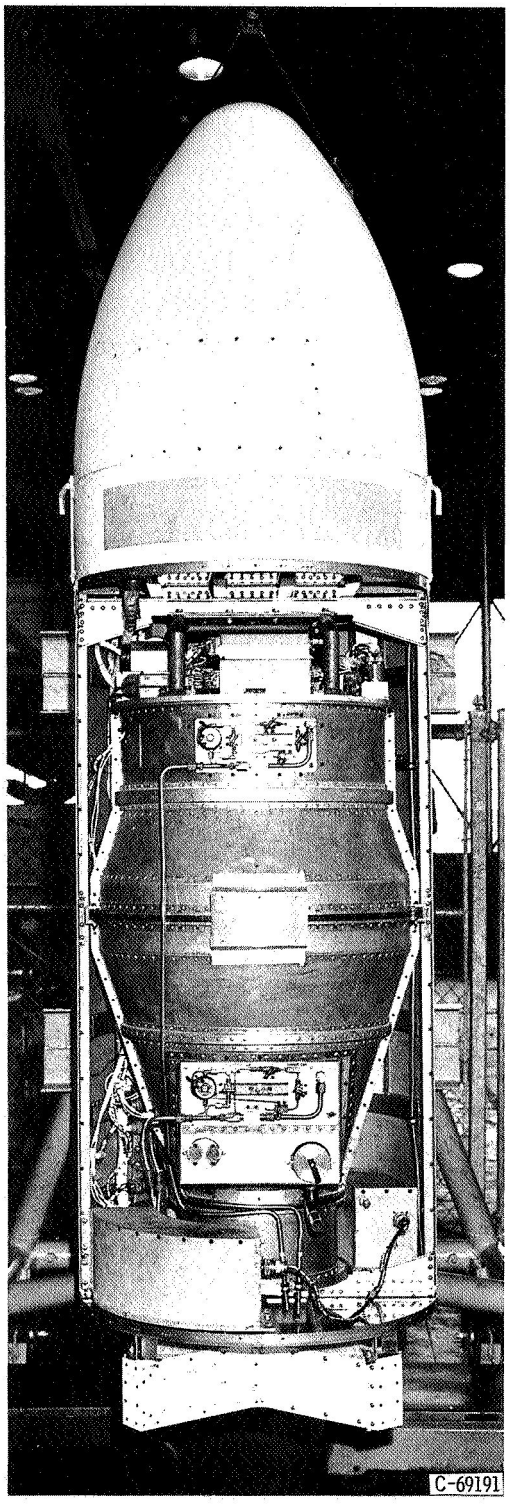

Figure 3. - Flight experiment mounted in scientific passenger pod.

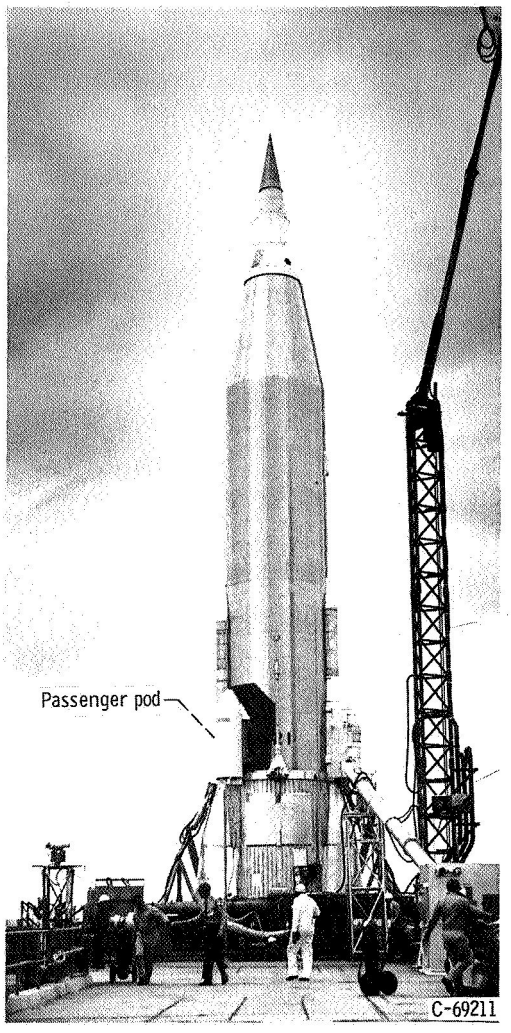

Figure 4. - Passenger pod mounted on Atlas missile.

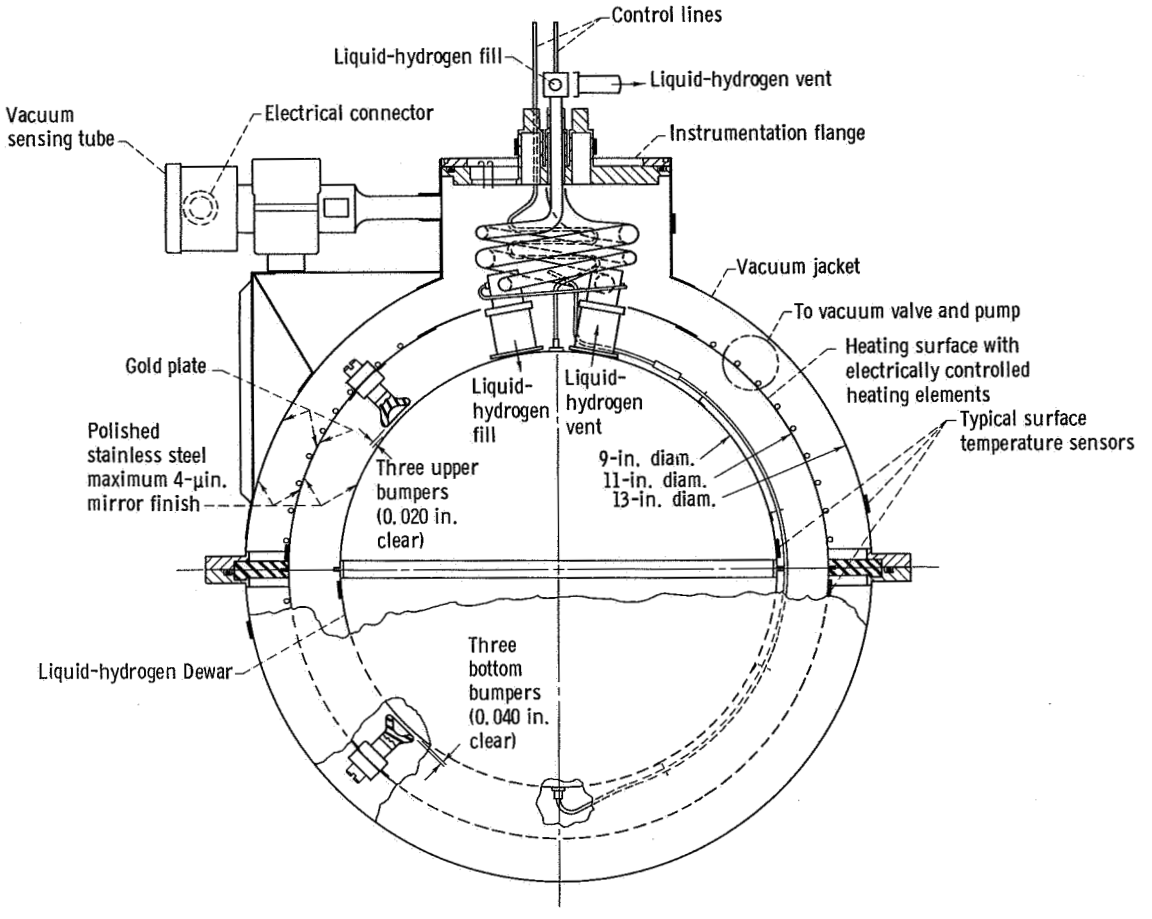

Figure 5. - Liquid-hydrogen Dewar.

constructed that heat shorts were minimized. The Dewar itself was suspended only by the fill, vent, and capillary lines shown schematically in figure 5. A photograph of a typical Dewar is presented in figure 7. The intermediate heater was supported by plastic rings cut out where possible to minimize conduction. Backup plastic support bumpers were located in the 45° planes to protect the Dewar during high acceleration and vibration periods, during shake tests, and during high-filling, liquid-nitrogen calibration tests. During normal testing and weightless flight, no contact was made with the bumpers. Figure 8 shows a heater with bumpers and a plastic support ring installed. The vacuum jacket, or outer sphere, contained the flanged vacuum seal as well as the pump line and the vacuum gage (see fig. 5). As shown in figure 5, the hemisphere flange is designed to restrain the plastic support ring holding the heater surface. The experiment parts were precleaned and assembled. After vacuum pumping the units were leak checked with a helium mass spectrometer prior to experimentation.

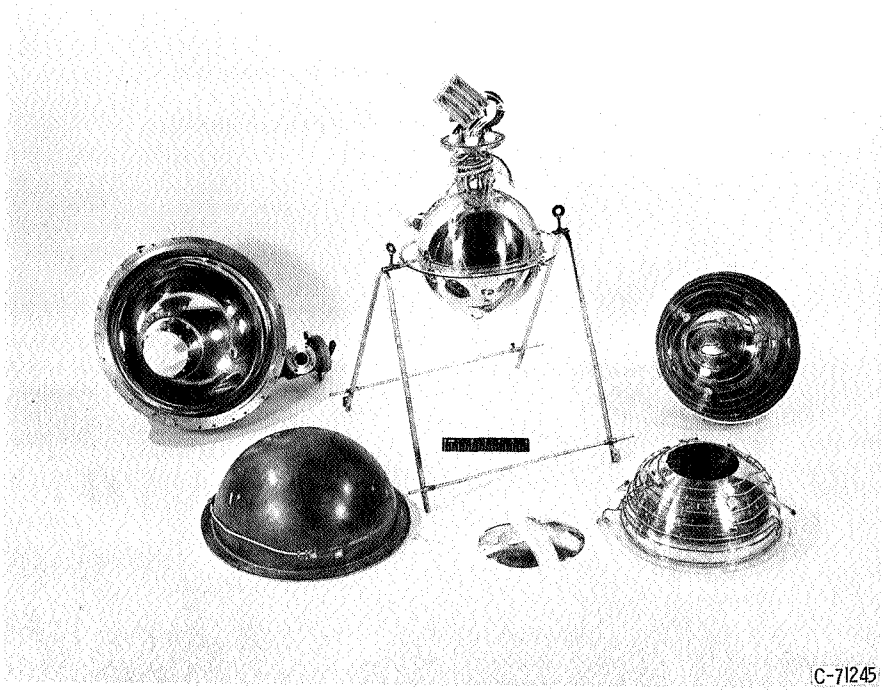

Figure 6. - Dewar assembly parts.

Experiment Housing and Pod Assembly

The experiment assembly was placed in an aluminum housing designed to contain both this Dewar and a larger but similar Dewar in a single unit (see fig. 1, p. 2). The experiment cryogenic and vacuum lines were connected to a control panel built into the housing as shown in figure 9. Included in this figure is a schematic flow diagram of the control panel. With this control panel the experiment operations, such as fill and vent, boiloff monitoring, liquid level control, pressure monitoring, and remote solenoid valve operation, could be accomplished. In addition to the relief valve shown in the diagram, a rupture disk was placed in the vacuum line as a safety precaution.

With the addition of the experiment electronics shelf, the experiments were installed in the passenger pod along with necessary associated hardware as shown in figures 10 (p. 9) and 3 (p. 4). The entire pod was approximately $8\frac{1}{2}$ feet long and 30 inches in diameter. The experiment section was approximately 5 feet in length. Besides the batteries, sequencer, and telemetry system, a mass stabilization system shown in figure 10 was included to attenuate any acceleration perturbation that might have been imparted by the vehicle or ejection mechanism. This system telescoped four weights, oriented 90° to the longitudinal axis of the pod and 90° from each other, to a distance of 50 feet each.

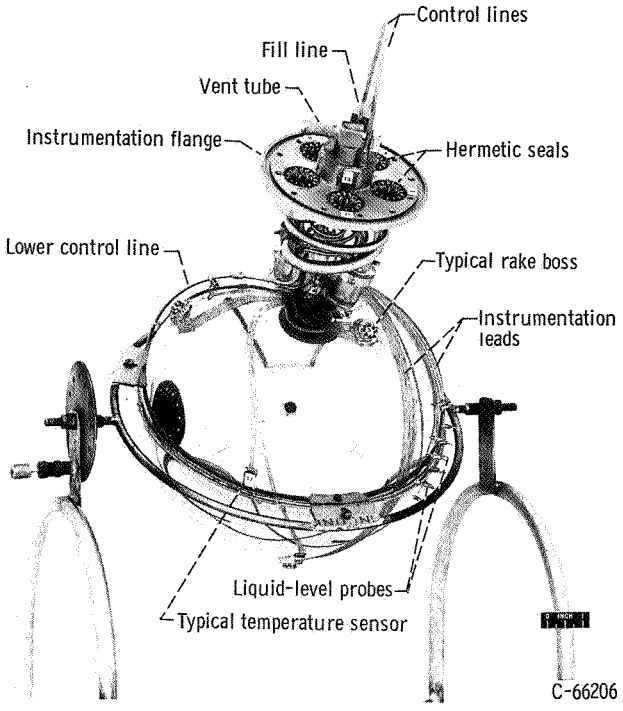

Figure 7. - Hydrogen Dewar and instrumentation.

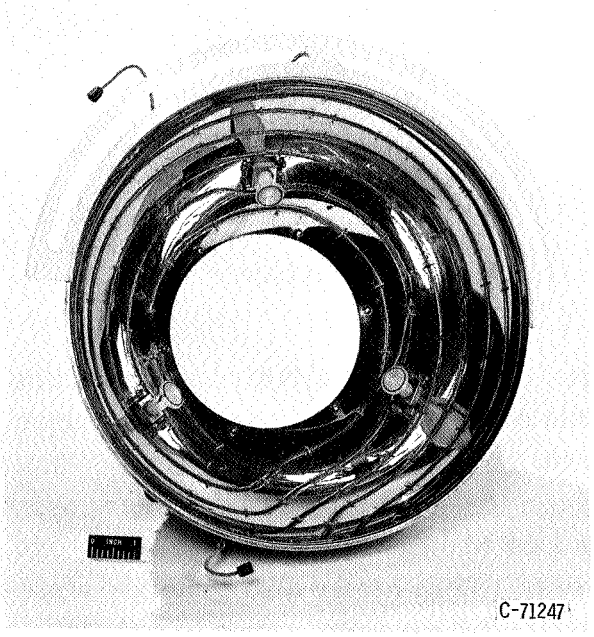

Figure 8. - Heater hemisphere with bumpers and support ring half.

Primary Experiment Instrumentation

The primary experiment instrumentation provided measurements of temperature, pressure, vacuum, and liquid level. Hydrogen Dewar wall temperatures were obtained by using platinum resistance sensors read by a Wheatstone bridge. These sensors were deposited platinum ribbon on a 1/4-inch-square sheet of ceramic (fig. 11, p. 9) bonded to the Dewar surface. A stainless-steel envelope was spot welded to the sphere wall over the sensor as a shield (fig. 7). Twelve sensors were discreetly located on the Dewar surface as sketched in figure 12 (p. 10).

In order to measure the liquid-hydrogen temperature profile and to determine the relative position of the gas ullage, four carbon resistor rakes, each containing four probes, were equispaced within the Dewar as shown in figure 12. Each probe was a 1/10-watt miniature composition resistor mounted on a hermetically sealed boss (fig. 11), which was soldered to the Dewar wall. At liquid-hydrogen temperatures, these resistors are extremely sensitive to temperature changes, and readily lend themselves to recording variations of tenths of degrees in bulk temperature with a Wheatstone bridge. The resulting narrow bridge range limited the temperature range of this system. Therefore, measurements made within the liquid were accurate within 0.1° R.

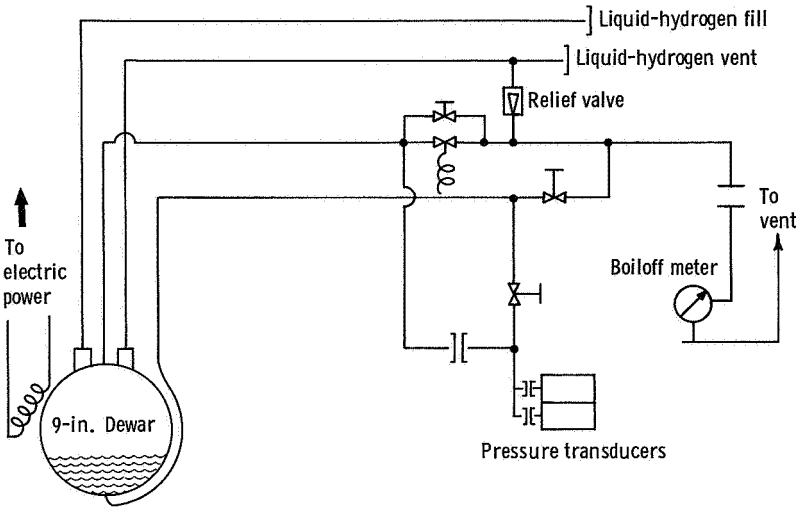

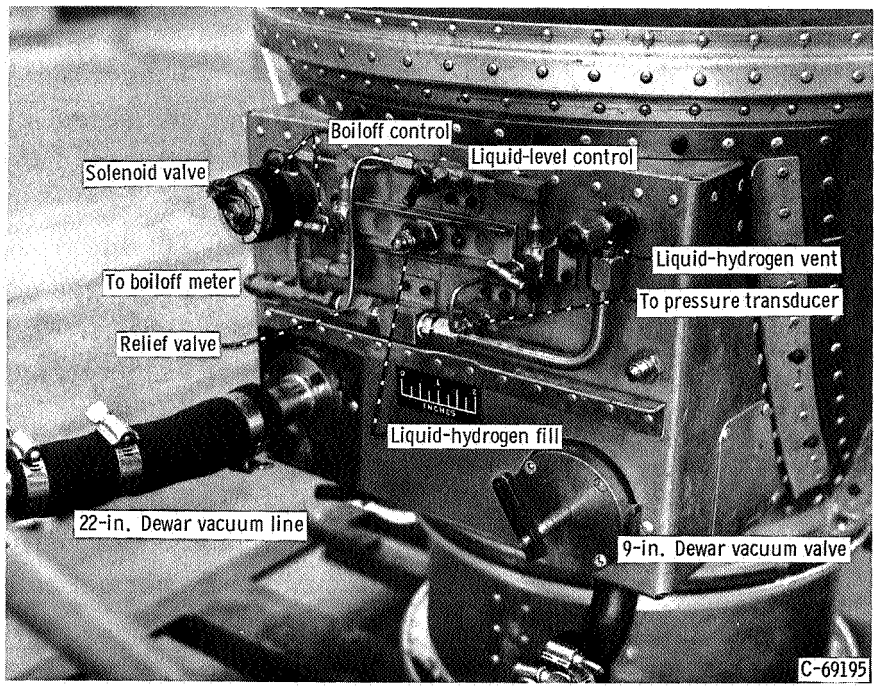

Figure 9. - Experiment control panel.

Measurements made outside the liquid, however, quickly became "off range." In this manner, therefore, the position of the gas bubble could be determined, while accurate temperature profiles of the liquid were measured.

The radiant heater shells were also instrumented with platinum resistance sensors. Each heater hemisphere contained five sensors located on an area-weighted basis, and their resistances were also read by bridge circuits. Each heater also contained a precisely calibrated wire-wound sensor used to control the electrical power to and, in turn, the temperature of the heater surface.

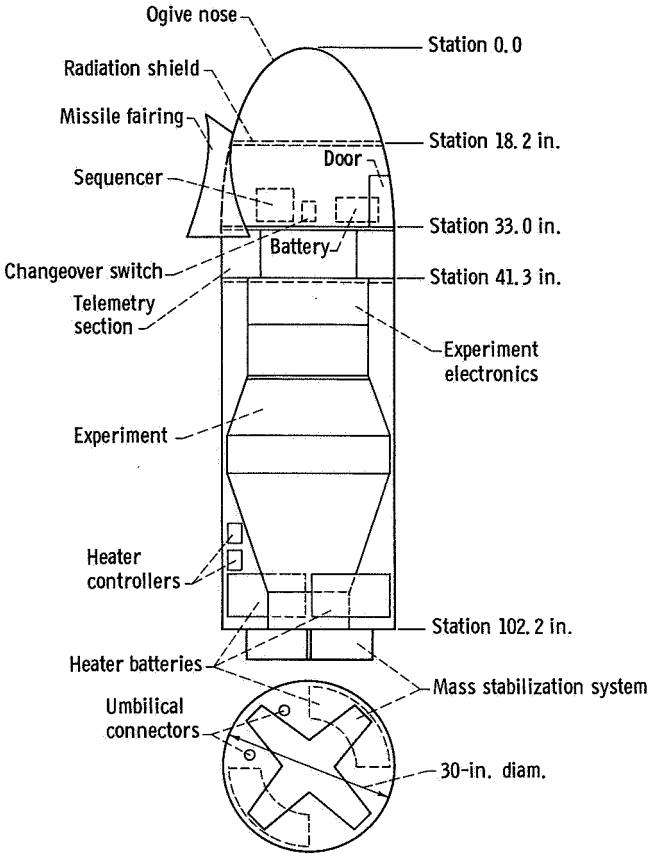

Figure 10. - Schematic of scientific passenger pod and experiments.

The hydrogen Dewar pressure was obtained with pressure-to-voltage transducers. Two separate units were used for reliability. The experiment vacuum was monitored with a readout power supply connected to the vacuum ionization gage (fig. 5, p. 5).

Liquid level prior to the flight was determined by a series of filament hot-wire probes mounted in the sphere as shown in figure 7. Each probe (fig. 11) consisted of a 0.001-inch-diameter filament wire approximately 3/16 inch long (depending on resistance match) through which about 300 milliamperes of current were pulsed. The liquid-covered filament indicated low resistance, while the vapor-covered filament indicated a considerable increase in resistance.

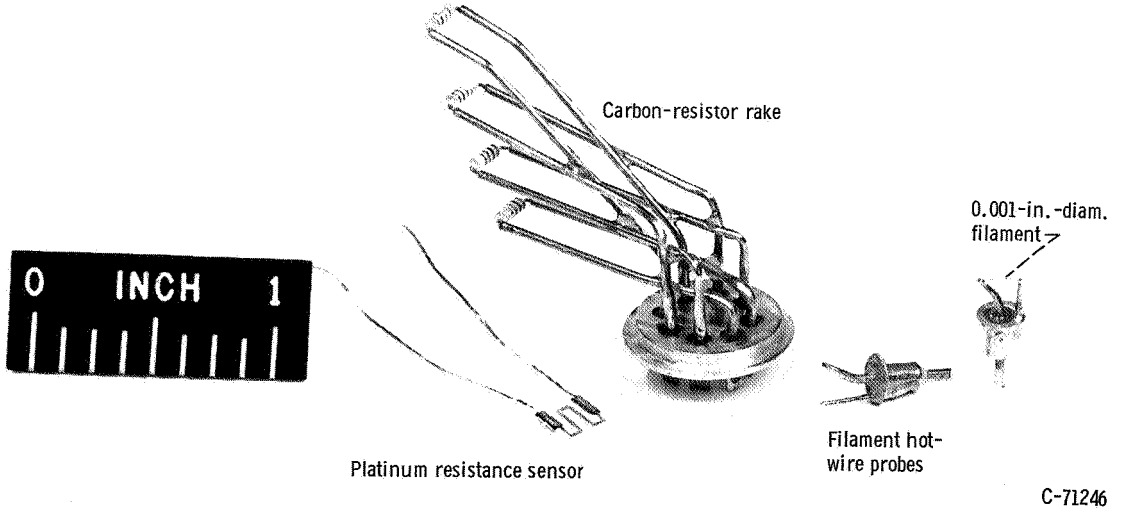

Figure 11. - Cryogenic instrumentation.

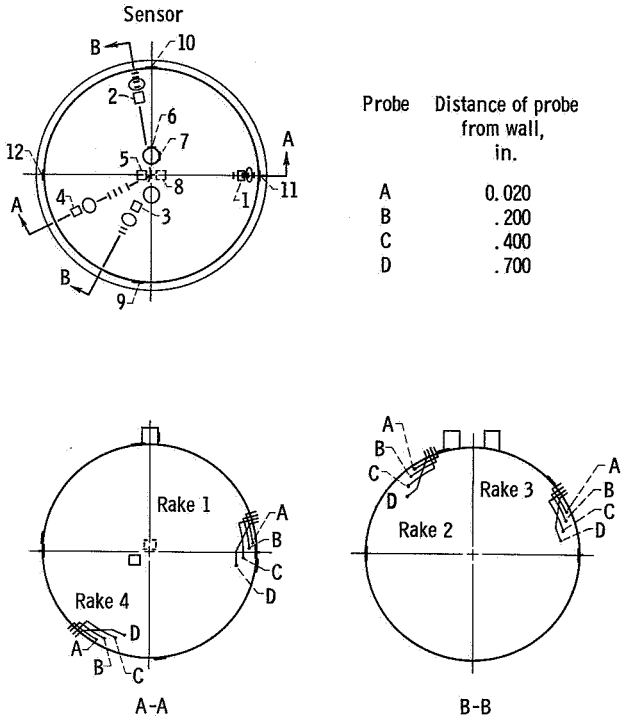

Probe	Distance of probe from wall, in.
A	0.020
B	.200
C	.400
D	.700

Figure 12. - Instrumentation location for liquid-hydrogen Dewar.

Flight Instrumentation

The flight instrumentation consisted of accelerometers, rate gyros, magnetic aspect sensors, signal conditioners, and a radiant-heater power supply and control circuit. General orientation of these instruments is depicted in figure 10, and the electronic instrument shelf is shown in figure 13.

Pod attitude and motion were determined by the use of the accelerometers, rate gyros, and magnetic aspect sensors. One 0.5- and one 0.01-g accelerometer were mounted in each axis to measure the accelerations affecting the experiment. Three rate gyros were mounted mutually perpendicular to indicate the roll rate in each of the three axes. The magnetic aspect sensors were also mounted to determine the relative position in the magnetic field of the Earth. The outputs of these instruments were wired to a high-level mechanical commutator and thus transmitted to the ground.

The signal conditioning equipment consisted of a temperature measuring system and an in-flight calibrator. The temperature measuring system consisted of a Wheatstone bridge to which each temperature sensor was mechanically commutated. The bridge output was amplified by a direct-current amplifier to a 0- to 5-volt signal and was telemetered. The in-flight calibrator interrupted the pressure transducer outputs periodically to calibrate the telemetry system.

The power to the radiant heaters was controlled by silicon-controlled rectifiers that were, in turn, controlled by the wire-wound sensors on each heater hemisphere. Each heater half was controlled individually.

Data Reduction

All test data were telemetered using six channels and were recorded on magnetic tape. The tapes were digitized at the Lewis Research Center. The data were then programed into data handling and computing equipment, along with the final calibrations and computing instructions.

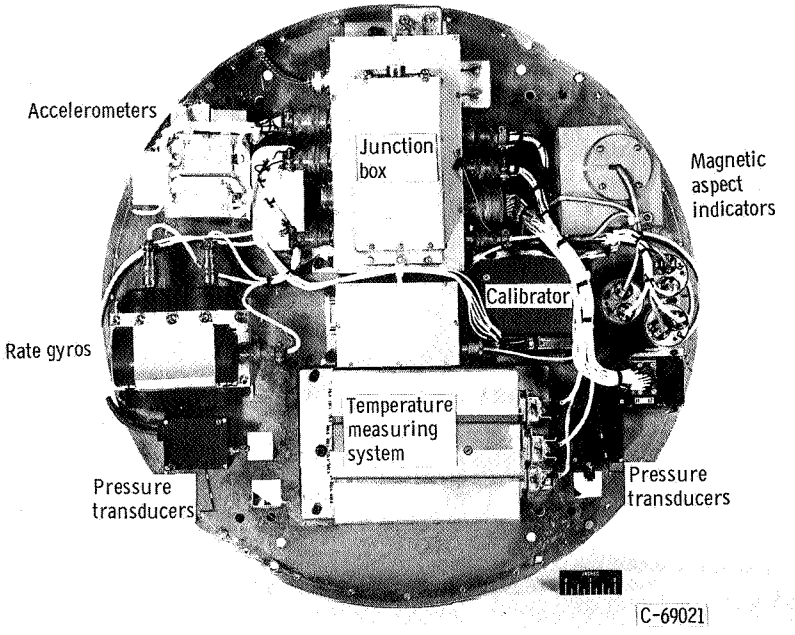

Figure 13. - Electronic instrument shelf.

PROCEDURE

The general procedure for all of the tests performed was as follows:

(1) Vacuum pumpdown

(2) Preliminary system checkout

(3) Chilldown

(4) Final calibrations

(5) Test performance

Usually the experiment Dewar was continuously vacuum pumped to reduce outgassing. While still connected to the pumping system, the experiment, including all instrumentation, was checked completely. At the same time, the cryogenic facility was inspected prior to operation. The Dewar was subsequently filled with liquid hydrogen to a level of 70 percent or greater, provided the initial vacuum was 0.5 micron of mercury or better. This high liquid filling augmented the Dewar chilldown period and rate. During this time, the boiloff of gaseous hydrogen was monitored as were the experiment temperatures and the vacuum. As the experiment vacuum was cryogenically pumped, the Dewar was removed from the pumping system. Ultimately, the vacuum prior to testing was usually of the order of 0.001 micron of mercury. When steady-state conditions prevailed, final calibrations of all transducers and sensors were taken and the experiment was ready to be tested.

For the homogeneous test the experiment was violently shaken. For this test the experiment prior to liquid filling was placed in a mechanical shaking rig. After calibrations, the liquid level was set to the desired percent of filling. Upon sealoff, shaking was initiated and data were taken. For the normal-gravity quiescent test the experiment remained stationary during testing. Test periods commenced with sealoff and continued for approximately 1/2 hour. Data were telemetered with an external ground transmitter and received by the Lewis telemetry station.

For the flight, test timing was critical because the launch time of the vehicle dictated the experiment liquid level. The general procedure was the same except that the entire operation was performed at the missile launch area complex. All preflight operations were performed according to a precise time schedule based on a predicted launch time. For the flight test all operations were performed while the experiment, along with another larger experiment, was contained within the pod. All instrumentation was monitored through the flight electronics and the hardline instrumentation by nearby checkout consoles. Telemeter checks were made with the pod telemeter by using external power. At a precise time in the preflight countdown, after final calibrations, the liquid level was so set that the percent filling at lift-off would be approximately 35 percent. This level was based on an expected boiloff from the time of pod mating to the vehicle until lift-off; a minimum time period of 4 hours was required. After mating to the missile, the hydrogen boiloff was monitored by television in the blockhouse. Instrumentation was monitored by equipment wired to the landlines through the umbilical connectors (fig. 10) and by way of the telemeter. At 45 seconds prior to lift-off the vent solenoid valve was closed to seal off the Dewar. At 30 seconds before lift-off the final liquid level was determined. At lift-off the umbilicals were pulled away and the in-flight heaters became operative.

After powered flight the pod was ejected from the missile, and the sequencer was timed to activate the mass stabilization system. During this time the pod should have been in a near zero-gravity environment, and the mass unit should have attenuated any powered-flight or ejection disturbances imparted to the pod. This weightless period was predicted to exist for approximately 1/2 hour before aerodynamic drag influenced the weightless liquid configuration. The pod was not monitored upon reentry, and no attempt was made to recover it.

FLIGHT CHARACTERISTICS

The experiment mounted in the passenger pod was launched piggyback on board an Atlas intercontinental ballistic missile (fig. 14). The detailed trajectory and flight characteristics cannot be presented; however, the general flight path and applicable events are shown in figure 15. This figure shows lift-off, powered flight, and pod

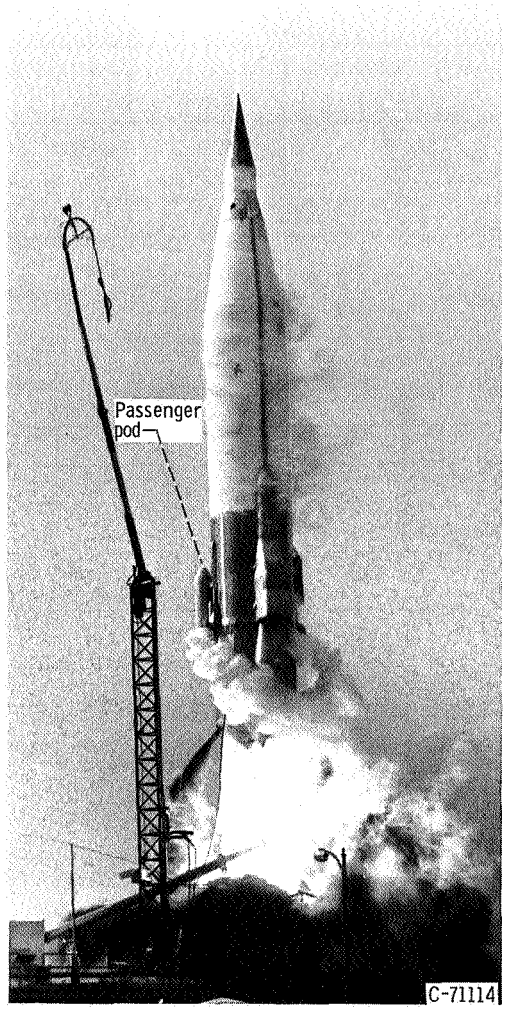

Figure 14. - Launch of passenger pod on board Atlas missile.

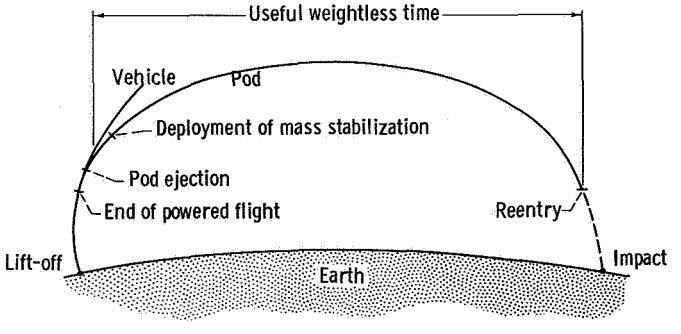

Figure 15. - Pod flight history.

ejection. At pod ejection the altitude was sufficient to permit a weightless environment. Fifteen seconds after the pod was ejected the sequencer was programed to switch power to the mass stabilization system. This system would attenuate any rotations or artificial accelerations imparted either by the boost vehicle or by the ejection itself. No power was received by the mass stabilizer, however, because of a malfunction in the circuit controlling the system.

The environment resulting from the vehicle platform and the ejection momentum may be obtained from the accelerometer and rate gyro data in figure 16. Figure 16(c) indicates the position of the accelerometers and gyros relative to the pod center of gravity and to the hydrogen Dewar. The dimensions indicate the relative multiplication effect at the hydrogen Dewar. As a result of these disturbances along the pod thrust axis and the multiplication effect, the liquid hydrogen experienced an acceleration field of about $10^{-3} \pm 0.25 \times 10^{-3}$ g that tended to force the liquid away from the center of gravity from approximately 8 minutes to 29 minutes after lift-off. During this 21-minute interval, the experiment was considered to be in a useful weightless environment. After this interval, aerodynamic drag affected the fluid configuration.

The oscillation period along the thrust axis was approximately 2 minutes while the period along the mutu-

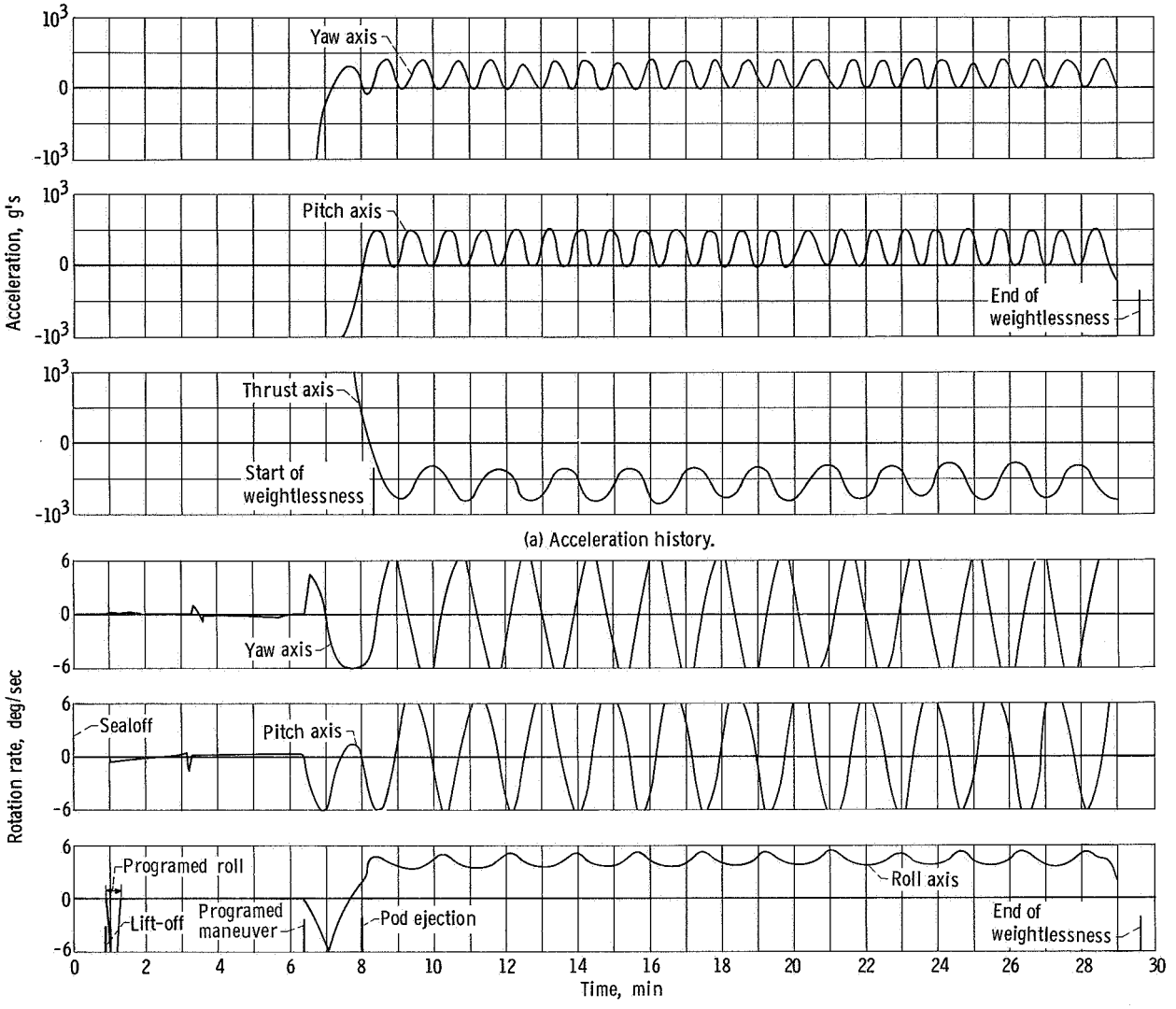

(a) Acceleration history.

(b) Rate gyro data.

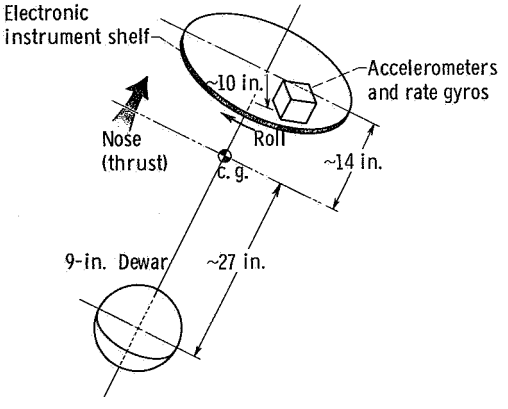

(c) Accelerometer and rate-gyro locations relative to Dewar and center of gravity of experiment pod.

Figure 16. - Flight characteristics.

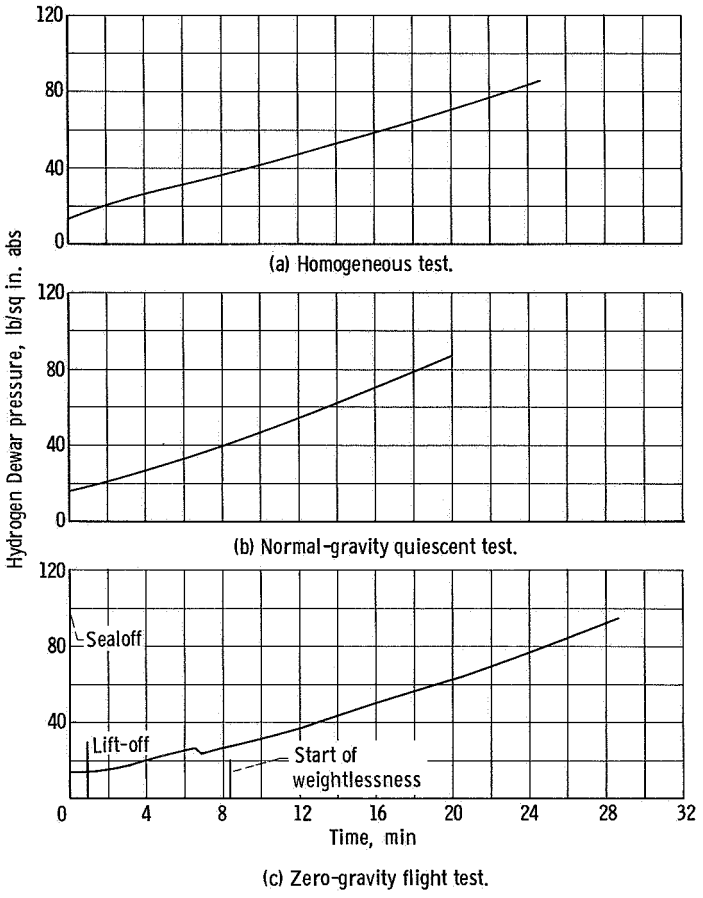

Figure 17. - Hydrogen Dewar pressure histories for homogeneous, quiescent, and zero-gravity tests.

ally perpendicular axes was 1 minute. As shown in figure 16(b), rate data from the gyros indicated that the pod was rotating about its longitudinal axis approximately 4° per second and tumbling end over end at a rate nearly 7° per second. The coupled effects of oscillatory motion about all the experiment axes affected the temperature readings, depending on the axis location of the respective sensors.

RESULTS AND DISCUSSION

Pressure Rise Characteristics

The configuration of the liquid hydrogen within the experiment container, coupled with the presence or absence of convection and buoyancy, grossly affects the heat-transfer and resulting pressure-rise characteristics of the system. Varying rates of pressure rise will be created whether the heat is added uniformly to the liquid and gas mixture, as for the homogeneous test, or is added fractionally to the liquid and gas. Each of these conditions existed for one or more of the test conditions presented in this report. For comparative purposes, therefore, two theoretical models are postulated, and curves of their respective pressure rise against heat added characteristics are used with the results of the actual tests. The first assumes homogeneous conditions throughout the fluid-vapor mixture, while the second assumes that all the heat added evaporates liquid. Equations developed from the first law of thermodynamics are presented in appendix B for both conditions, and the resulting curves are included with the test data for comparison. (Symbols are defined in appendix A.)

For the three tests performed with the experiment, the homogeneous test, the normal-gravity quiescent test, and the near zero-gravity flight test, the resulting actual pressure-rise data plotted against time are shown in figure 17, and the corresponding heater temperature histories are plotted in figure 18. As may be seen for the heater temperature curves, seal-off, or beginning of a test, was initiated when the

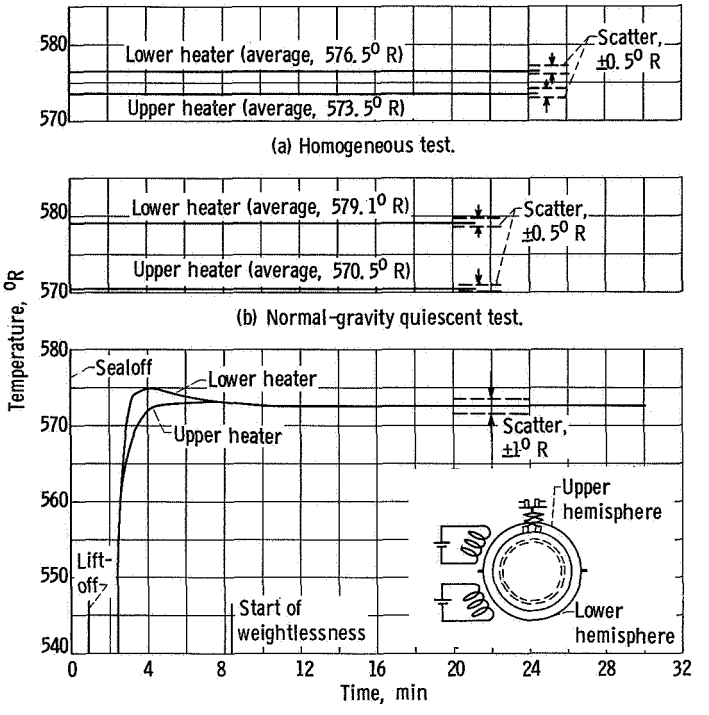

Figure 18. - Heater temperature histories for homogeneous, quiescent, and zero-gravity tests.

heaters were up to control temperature for both normal-gravity tests, while the heaters were started at lift-off for the flight test.

The total heat added to the hydrogen was computed on the basis of the heater temperatures. The development is made in appendix B, and the results are plotted as a function of measured pressure in figure 19(a). The two theoretical models for homogeneous and surface evaporation conditions are included for reference. Since none of the tests were performed at precisely the same liquid filling, the variation of the respective theoretical comparison curves depended on the filling. For convenience, then, the pressures as a function of heat added were replotted in figure 19(b) by using the percent pressure deviation as the common comparison. The percent pressure deviation (at a particular heat added) is defined as the percentage above homogeneous pressure that an actual experimental data point is between the homogeneous and the surface evaporation lines. That is,

Percent pressure deviation

$$\equiv \left[\frac{\text{(actual pressure) - (homogeneous pressure)}}{\text{(surface evaporation pressure) - (homogeneous pressure)}}\right]_{Q_i} \times 100$$

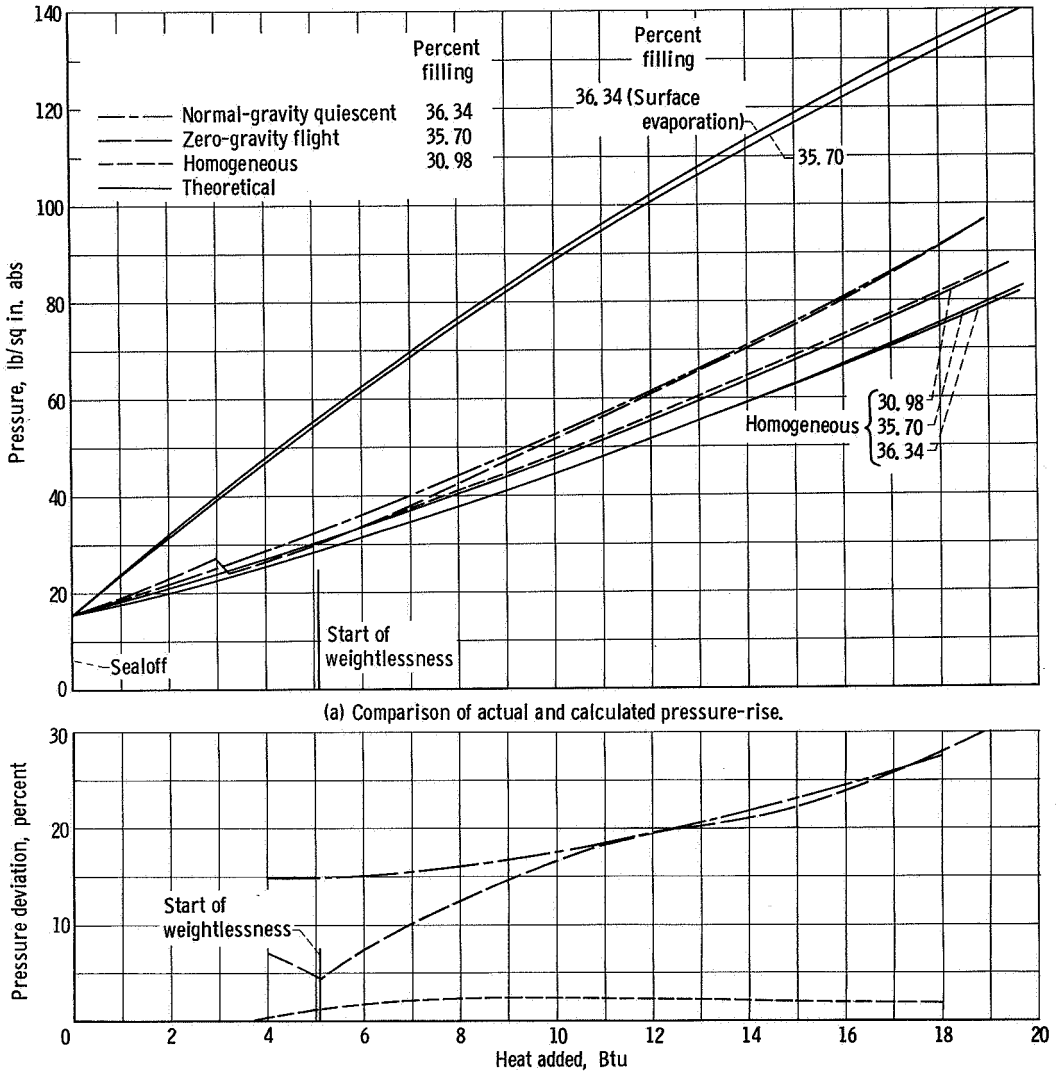

(a) Comparison of actual and calculated pressure-rise.

(b) Percent deviation of actual pressures from surface-evaporation and homogeneous pressures.

Figure 19. - Pressure-rise characteristics with heat added for homogeneous, normal-gravity quiescent, and zero-gravity flight tests.

Since the actual homogeneous test approximated the theoretical line for a uniform (homogeneous) mixture, a comparison of the experimental data with the computed theoretical line is indicative of the experimental system accuracy of the tests. Comparing, then, the shake test data and the theoretical homogeneous curve (fig. 19(b)) for the same filling, 30.98 percent, shows a maximum pressure deviation of 2.5 percent.

As may be seen in figure 19(b), the normal-gravity quiescent data show a gradual deviation toward surface evaporation ranging from 15 to nearly 30 percent. The flight data, on the other hand, started at less than 5 percent at the beginning of weightlessness, rapidly approached the quiescent level, and maintained nearly the same rise rate during

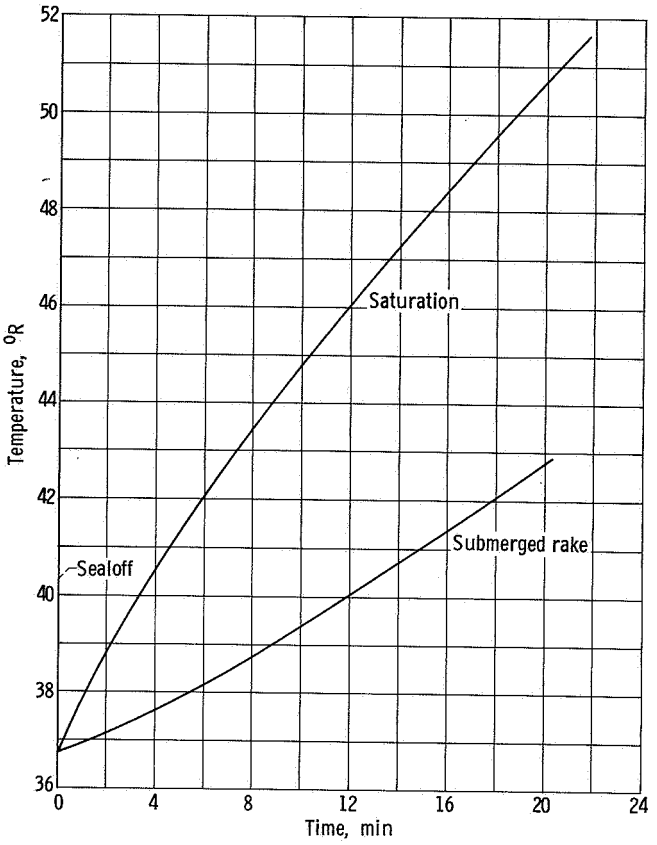

Figure 20. - Stratification during normal-gravity quiescent test.

the remainder of the test period. The initial transients experienced during missile boost and pod ejection are not shown in figure 19(b) because they are of no value to the particular problem under investigation. The reason for the near homogeneous starting point for the flight curve, however, was the result of the mild mixing action due to ejection momentum.

Temperature Profiles

Bulk temperature profiles, including values from probes in the liquid-gas interface and Dewar surface temperatures, were obtained by using the series of four temperature rakes equally spaced within the Dewar and the 12 surface sensors, as described in figure 12. The rakes served a dual purpose, both that of measuring temperature profiles and also that of locating the interface. The combination of rake and wall temperatures, then, should provide a fairly accurate description of the fluid configuration. For the homogeneous shake test, of course, all this instrumentation indicated saturated temperatures as dictated by measured pressure, and, therefore, the temperatures are not presented. For the normal-gravity quiescent test, one rake was submerged in liquid while the remaining three were above the liquid level. The temperature history for the submerged rake is shown in figure 20; however, the remaining rake temperatures were off range of the temperature measuring system. Manually recorded data for the surface sensors (fig. 21) indicate degree of superheating above the liquid level and subcooling below the liquid. Generally, the farther above the liquid level, the higher the temperature. Of particular significance is the amount of subcooling indicated both by the submerged rake (fig. 20) and by the wall sensors below the liquid (numbers 4 and 8, fig. 21). Subcooling by as much as 7° R was reached at the end of testing, approximately 20 minutes after sealoff.

The temperature profiles measured during the flight test are presented in figure 22 for the rakes and in figure 23 for the surface sensors. The data for rakes 1, 2, and 3

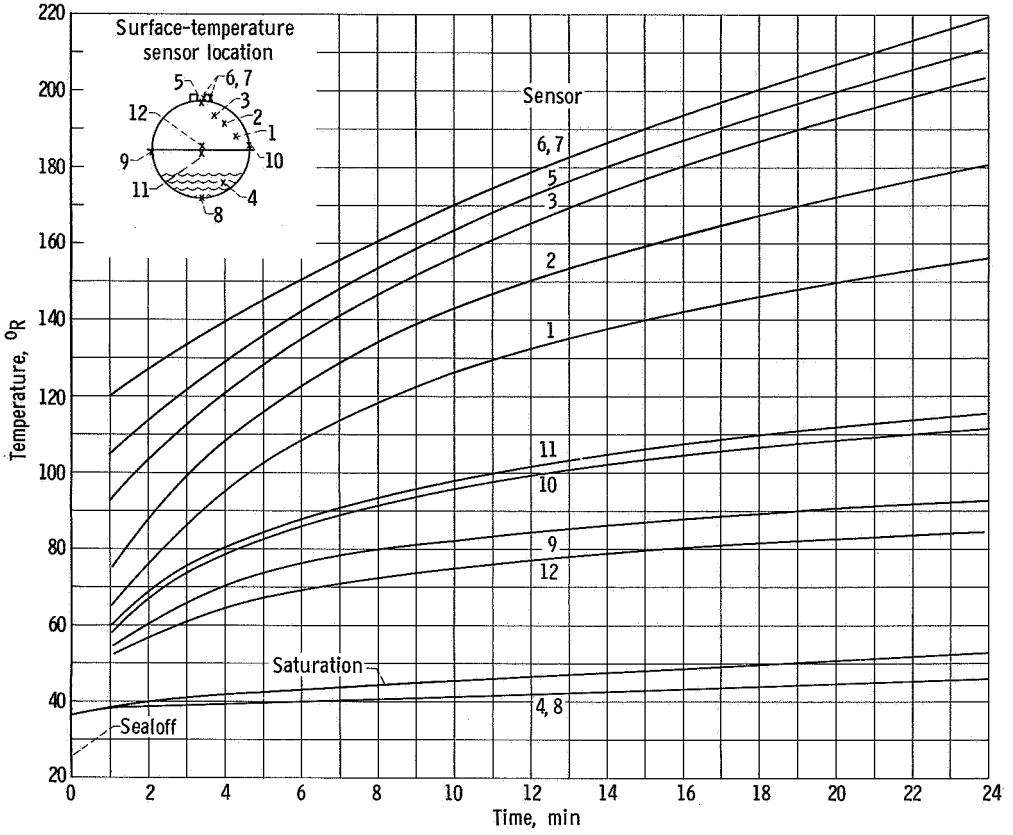

Figure 21. - Typical hydrogen Dewar surface temperatures during normal-gravity quiescent test.

are in figures 22(a), (b), and (c), respectively, while the data for rake 4 are plotted individually in figure 22(d) for each probe because the oscillations in the traces would make superposition difficult to analyze. The relative locations of the rakes shown out of true plane are indicated in the sketch in figure 22(a). The oscillations in the data may be correlated with the acceleration perturbation data of figure 16 and are of the same frequency for the same planar location of the rake. Two significant results may be obtained from these data, however. First, the magnitude of subcooling for the weightless configuration was approximately 1° to 3° R when oscillations were not included and as much as 6° R when the perturbation cycling during the "on-range" time of the temperature sensors during flight was taken into account. Second, fluid location within the Dewar may be predicted. Since the rake probes were so placed that each resistor would be liquid-wetted for a perfectly centered ullage, nonuniform rake temperatures indicate eccentricity of the fluid configuration. Study of the temperature profiles of figure 22 imply that the liquid hydrogen was not uniformly located along the Dewar surface. That area near the fill-vent contained a thinner liquid depth than did the rest of the surface, perhaps as shown in the sketch in figure 22. This depth is indicated by the temperature history of rake 3 (fig. 22(c)); the temperatures of probes D and C increased rapidly later in the flight and crossed the saturation curve, indicating vapor wetting.

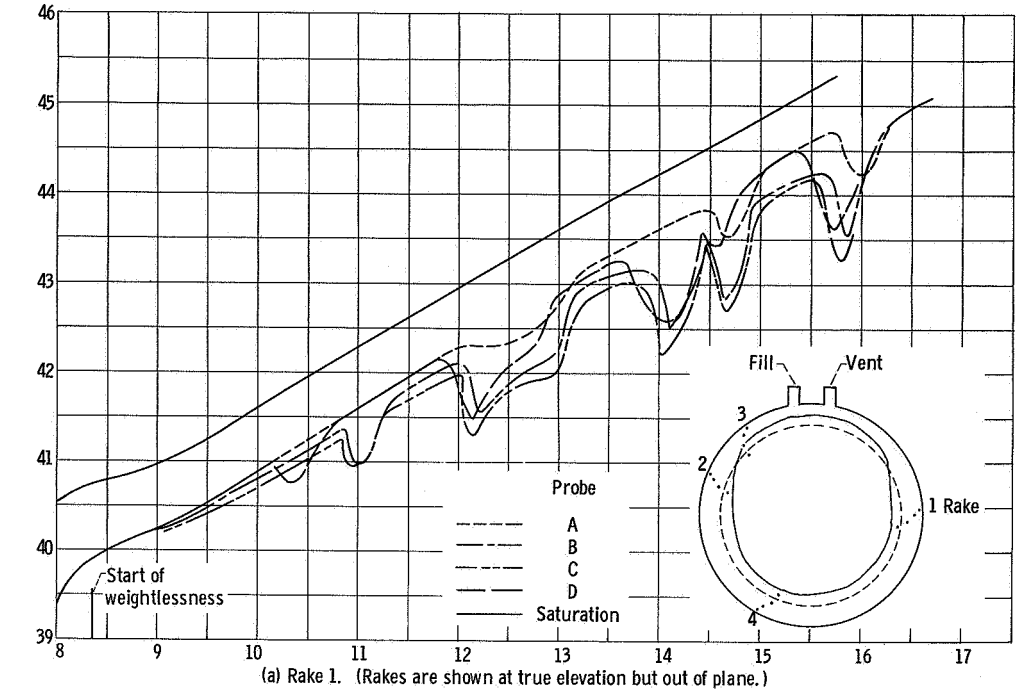

(a) Rake 1. (Rakes are shown at true elevation but out of plane.)

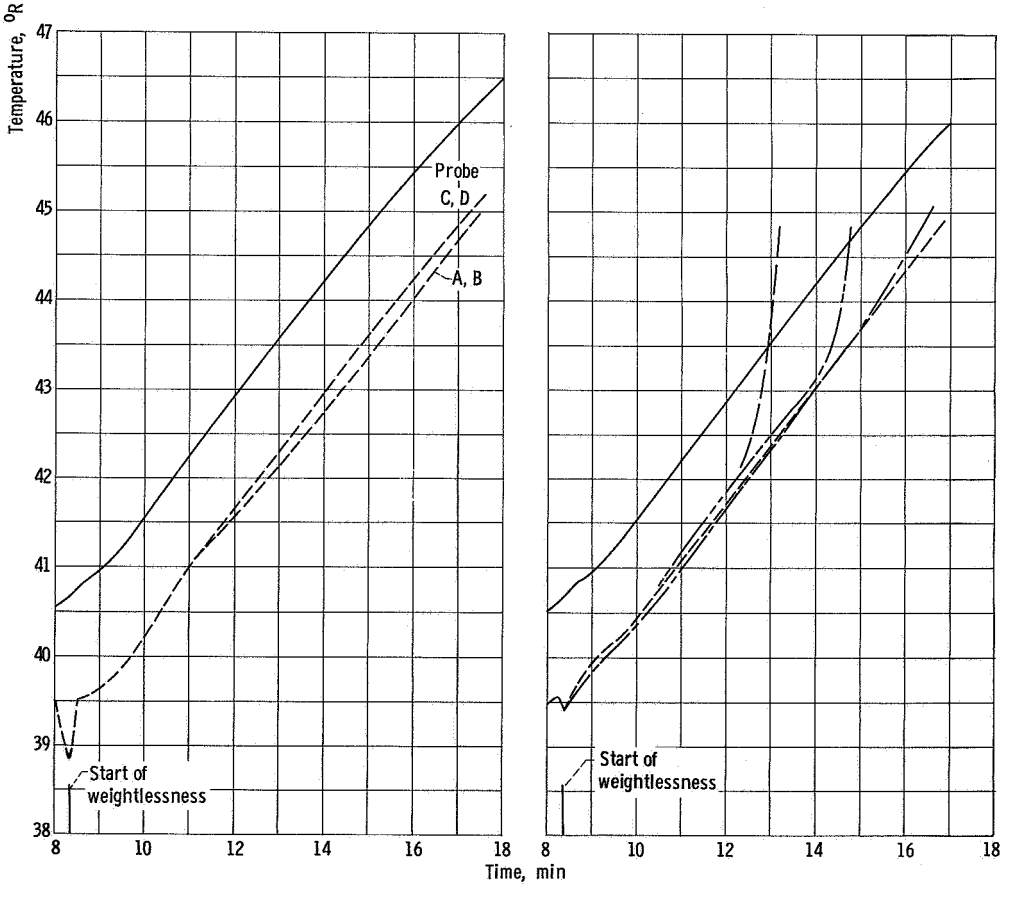

(b) Rake 2.

(c) Rake 3.

Figure 22. - Hydrogen temperature profiles during flight test.

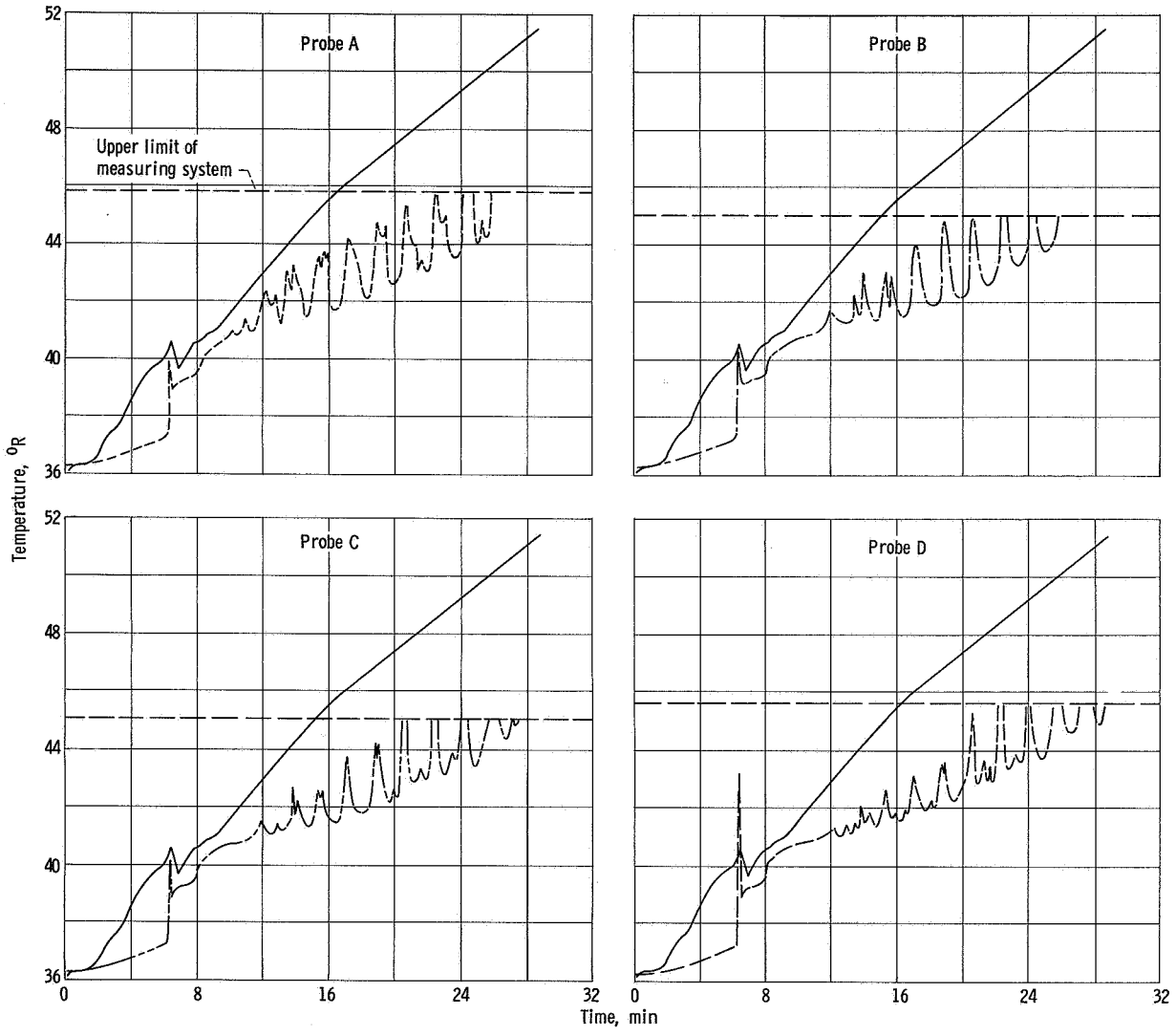

(d) Rake 4.

Figure 22. - Concluded.

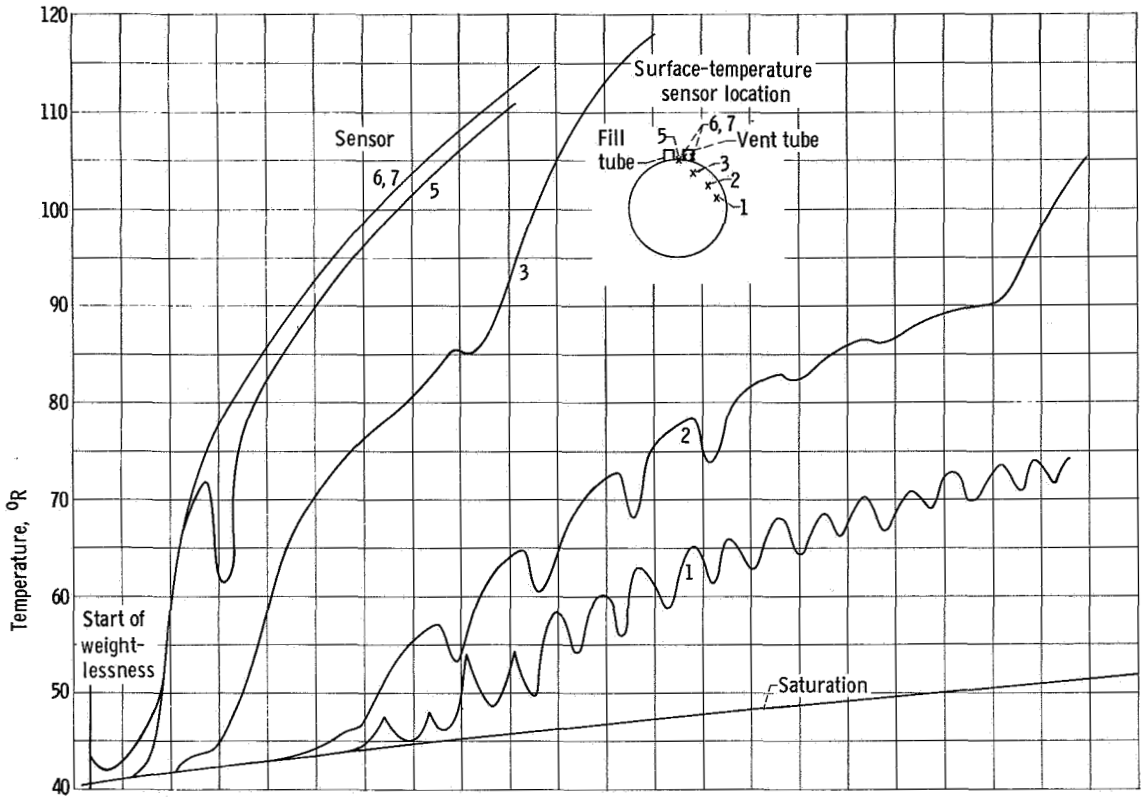

(a) Temperature sensors near fill and vent tubes.

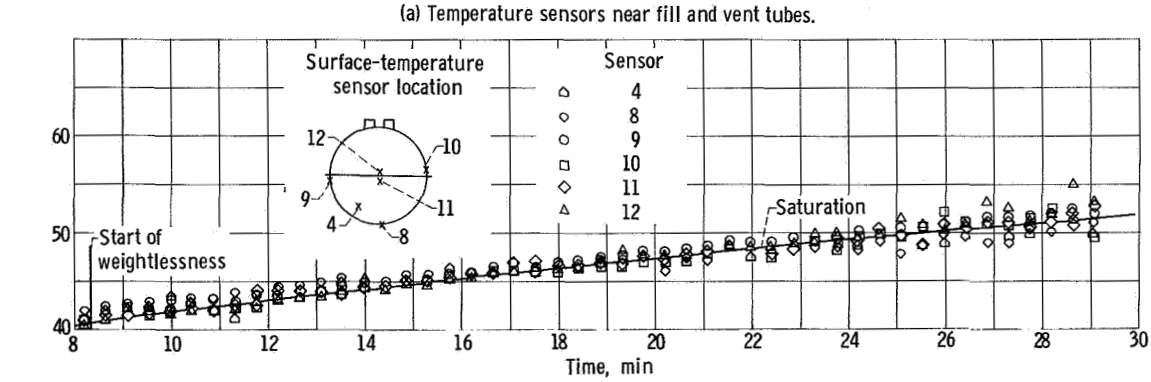

(b) Temperature sensors near meridian and side opposite fill and vent tubes.

Figure 23. - Hydrogen Dewar surface temperatures during zero-gravity flight test.

Study of the acceleration data also shows that this is the direction of the induced gravitational field; that is, the liquid is pulled away from the fill-vent area of the Dewar.

Wall Drying Phenomenon During Flight Test

Within 1 minute after the inception of the weightless period, wall drying started at the point of greatest heat leak (sensor 5 at the fill and vent tubes), as indicated by the temperature response in figure 23(a). This area of the Dewar also contained the thinnest

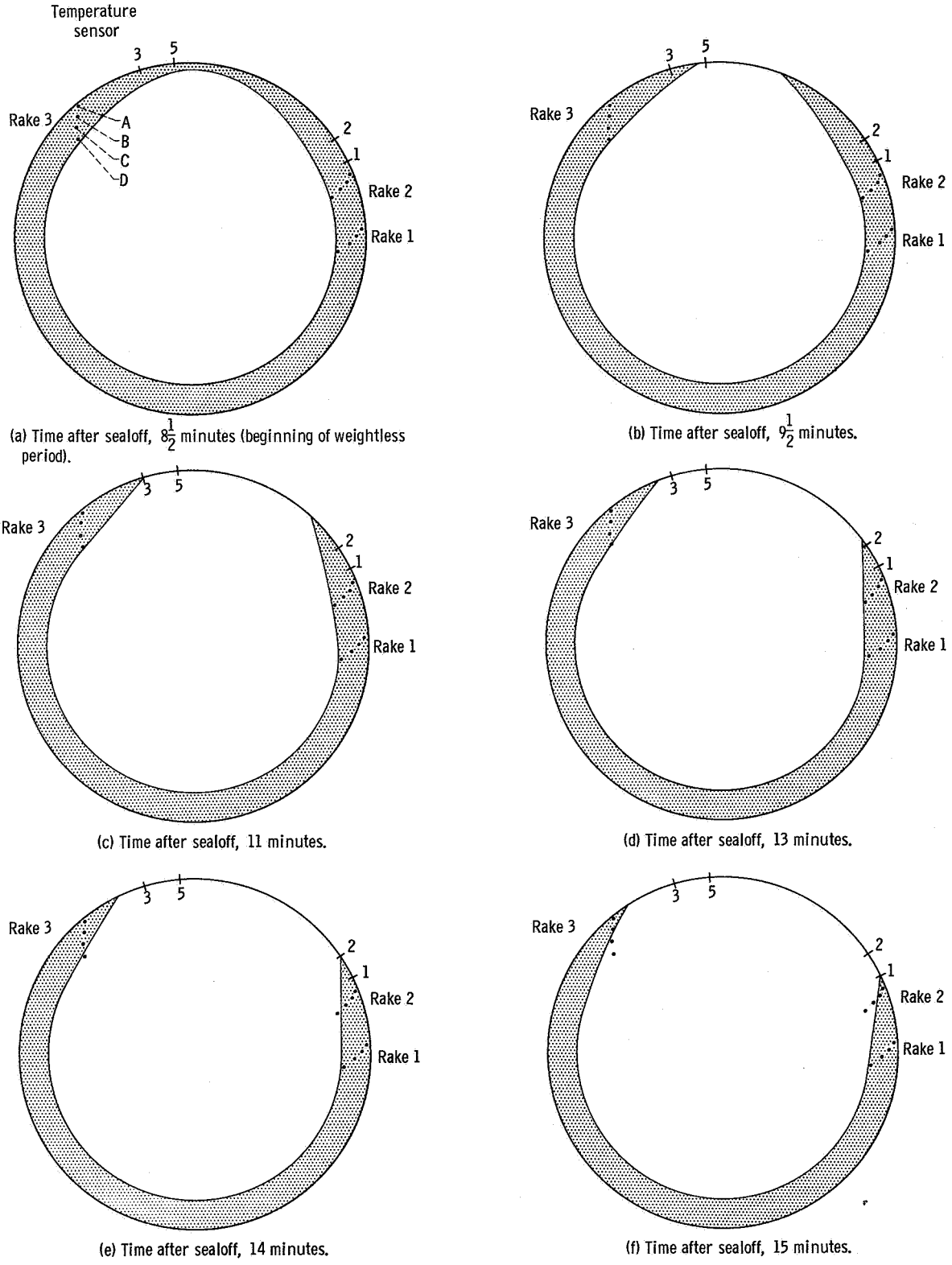

(a) Time after sealoff, $8\frac{1}{2}$ minutes (beginning of weightless period).

(b) Time after sealoff, $9\frac{1}{2}$ minutes.

(c) Time after sealoff, 11 minutes.

(d) Time after sealoff, 13 minutes.

(e) Time after sealoff, 14 minutes.

(f) Time after sealoff, 15 minutes.

Figure 24. - Liquid configurations during weightless period. (All sensors and probes are shown at true elevation but out of plane.)

liquid depth, as indicated by the rake data in figure 22. This wall drying progressed (see fig. 23(a)) toward the sphere meridian, as indicated by sensors 3, 2, and 1. The wall temperatures along either side of the meridian and on the opposing hemisphere generally indicated approximately saturated conditions (fig. 23(b)).

CONCLUDING REMARKS

The results of the pressure rise characteristics, although indicating similar trends between normal-gravity quiescent and low-gravity flight tests, may be explained by considering the actual flight conditions and the wall-drying phenomenon. The flight was characterized by a residual rotation in all three principal axes of the pod and experiment. This rotation created, with reference to the experimental Dewar, an undesired acceleration field with a magnitude at the Dewar of approximately 10^{-3} g in a direction tending to force the liquid away from the fill and vent area of the container. The force field was not sufficient to destroy the weightless configuration (gas ullage within a liquid envelope), as is evident from the rake data, but was sufficient for small convection and buoyant forces to be present. It is believed, then, that the configuration at the beginning of the weightless period approximated that shown in figure 24(a). Within the following minute the area at the fill and vent tubes had dried as outlined in figure 24(b). Figures 24(c), (d), (e), and (f) indicate the progression of drying past the respective wall sensors and also crossing probes D and C of rake 3. As figure 24 shows, the drying did not progress uniformly in reference to the longitudinal axis. This nonuniformity is probably the combined effect of the resultant axis of rotation and the surface tension baffle characteristics (ref. 1) of the rake probes. That is, the rake probes, in acting like a position controlling baffle, tended to distort the weightless configuration and perhaps delay the time before a particular probe became vapor wetted. Drying past rake 2 was not indicated during the time of "on-range" data recording.

The results of this drying phenomenon, therefore, provide a mechanism, similar to the normal-gravity quiescent test, by which heat may be added directly to the vapor and/or liquid-vapor interface. This type of heating will tend to bring the actual pressure rise closer to the surface evaporation theoretical line. Because of these particular conditions, the near zero-gravity pressure rise, as shown in figure 19 (p. 17), approximated that obtained during the normal-gravity quiescent test.

SUMMARY OF RESULTS

As a result of mass stabilization system failure, an artificial acceleration field

was present throughout the flight test such that the hydrogen Dewar experienced a force of $10^{-3} \pm 0.25 \times 10^{-3}$ g while rolling approximately 4° per second and tumbling nearly 7° per second. Under these conditions for the zero-gravity flight test, pressure rise characteristics compared with the homogeneous and normal-gravity quiescent tests for a liquid-hydrogen Dewar indicate the following results:

1. The weightless configuration was not centered during the flight test, as indicated by rake temperatures, resulting in varying liquid depths dictated by the artificial acceleration.

2. A wall-drying phenomenon prevailed during the flight test in the Dewar area where the heat leak was greatest and the liquid layer thinnest (because of rotation).

3. The pressure rise characteristics for the near zero-gravity flight test were approximately equivalent to those for the normal-gravity quiescent test. This was apparently the result of similarity in the heat-transfer models arising from the flight perturbations and wall drying.

4. During flight the temperature rakes indicated cyclic variation in liquid temperature, in phase with the perturbation frequencies. As much as 6° R subcooling was measured compared to 7° R for the normal-gravity quiescent test.

Lewis Research Center,
National Aeronautics and Space Administration,
Cleveland, Ohio, February 19, 1965.

APPENDIX A

SYMBOLS

A	surface area, sq ft
B_{il}	absorption factor
F	angle factor
c_p	specific heat, Btu/(lb)(^oR)
k	thermal conductivity Btu/(hr)(ft)(^oR)
k_m	mean thermal conductivity, Btu/(hr)(ft)(^oR)
L	length, ft
m	mass, lb
P	pressure, lb/sq in. abs
Q	total heat, Btu
q	heat addition rate, Btu/hr
r	reflectivity
T	absolute temperature, ^oR
t	time
U	total internal energy of system Btu
u	specific internal energy, Btu/lb
V	volume, cu ft
v	specific volume, cu ft/lb
W	mass of hydrogen container, lb
ϵ	emissivity
ρ	density, lb/cu ft
σ	Stefan-Boltzmann constant, 0.1713×10^{-8} Btu/(hr)(sq ft)(^oR)^4

Subscripts:

a	absorbed
f	final or any intermediate state
gc	gaseous conduction
in	initial state
ℓ	liquid
r	radiant
s	system
sc	solid conduction
st	stored
v	vapor
1, 2, 3	heat-transfer surfaces

APPENDIX B

THERMODYNAMIC AND HEAT-TRANSFER CALCULATIONS

The calculations used to analyze the data of this experiment were divided into two parts, thermodynamic calculations and heat-transfer calculations. The thermodynamic calculations produced theoretical results needed to generate curves of pressure against heat added to the experiment. The actual curves of pressure against heat added were obtained by using the heat-transfer calculations with values of data taken from the experimental tests.

Thermodynamic calculations

The experiment is considered to be a nonexpanding closed system of which the only energy input is in the form of heat. Thus, from the first law of thermodynamics

$$Q = \Delta U + P\,dV \tag{1}$$

where

$$P\,dV \approx 0$$

It is assumed that the initial state of the system can be described as a homogeneous mixture of liquid and vapor existing at saturation temperature and atmospheric pressure. The percent filling at the start of the test is also known. Thus equation (1) may be written

$$Q = U_f - U_{in} \left(m_{\ell,f} u_{\ell,f} + m_{v,f} u_{v,f}\right) - \left(m_{\ell,in} u_{\ell,in} + m_{v,in} u_{v,in}\right) \tag{2}$$

where the subscripts in and f designate, respectively, the initial and final states of the system. Since the system in the initial state is homogeneous and is at the saturated temperature corresponding to atmospheric pressure, the specific volume and specific internal energy can also be found at this state:

$$m_{\ell,in} = \frac{V}{v_{\ell,in}} \left(\frac{\text{percent filling}}{100}\right)_{in} = \rho_{\ell,in} \left(\frac{\text{percent filling}}{100}\right)_{in} V \tag{3}$$

$$m_{v,\,in} = \frac{V}{v_{v,\,in}} \left(\frac{\text{1-percent filling}}{100} \right)_{in} = \rho_{v,\,in} \left(\frac{\text{1-percent filling}}{100} \right)_{in} V \tag{4}$$

The total internal energy at the initial state can now be determined, using properties given in reference 28.

For a nonexpanding, closed system the mass of the liquid plus the mass of the vapor is a constant value and is equal to the mass of the system. Thus, the system density is also constant, and

$$\rho_s = \left(\frac{\text{percent filling}}{100} \right)_{in} \rho_{\ell,\,in} + \left(1 - \frac{\text{percent filling}}{100} \right)_{in} \rho_{v,\,in} \tag{5}$$

When the homogeneous model is considered in the final state, the density and internal energy of each phase can be determined because the homogeneous mixture exists at the saturation temperature corresponding to the final system pressure. From equation (5) the percent filling at the final state is

$$\left(\frac{\text{percent filling}}{100} \right)_f = \frac{\rho_s - \rho_{v,\,f}}{\rho_{\ell,\,f} - \rho_{v,\,f}} \tag{6}$$

As in the initial state, the total energy at the final state can easily be found because

$$m_{\ell,\,f} = \rho_{\ell,\,f} \left(\frac{\text{percent filling}}{100} \right)_f V \tag{7}$$

$$m_{v,\,f} = \rho_{v,\,f} \left(1 - \frac{\text{percent filling}}{100} \right)_f V \tag{8}$$

Thus, all the terms of equation (2) are now known, and the amount of heat needed to reach the final state of the homogeneous model can now be calculated.

A second set of theoretical conditions is obtained in the surface evaporation model, which will now be considered. The initial state of this model is identical to the initial state of the homogeneous model, and all the thermodynamic properties of this state are calculated identically. It is assumed in this model, however, that all of the input energy is used to evaporate the liquid, so that the density and specific internal energy of the remaining liquid is unaltered by this heat-exchange process, and that the density and specific internal energy of the homogeneous vapor are defined by the saturated temperature and the final system pressure:

$$\rho_{\ell,\,in} = \rho_{\ell,\,f} \quad \text{and} \quad u_{\ell,\,in} = u_{\ell,\,f} \tag{9}$$

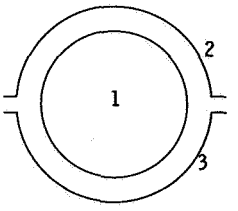

Figure 25. - Heat-transfer surfaces of intermediate and inner spheres.

$$\left(\frac{\text{percent filling}}{100}\right)_f = \frac{\rho_s - \rho_{v,\,f}}{\rho_{\ell,\,in} - \rho_{v,\,f}} \tag{10}$$

$$m_{\ell,\,f} = \rho_{\ell,\,in}\left(\frac{\text{percent filling}}{100}\right)_f V \tag{11}$$

$$m_{v,\,f} = \rho_{v,\,f}\left(1 - \frac{\text{percent filling}}{100}\right)_f V \tag{12}$$

The total internal energy at the final state can now be determined, and the total amount of heat required to reach the final state can again be calculated by equation (2).

Heat-Transfer Calculations

The heat absorbed by the contained hydrogen is equal to the sum of the heat transferred by radiation (from the heaters), the heat transferred by solid conduction (through the vent tubes and wires), and the heat transferred by gaseous conduction minus the heat stored in the container itself:

$$\Delta Q_a = (q_r + q_{sc} + q_{gc})\Delta t - \Delta Q_{st} \tag{13}$$

With the notation shown in figure 25, the heat transferred by radiation from surfaces 2 and 3 (the radiation heaters) to surface 1 is determined by the method presented in reference 29. The net rate of radiant heat absorbed by surface 1 is given by

$$q_1 = \sum_{i=1}^{3} \sigma B_{i,\,1}\epsilon_i A_i T_i^4 - \sigma\epsilon_1 A_1 T_1^4 \tag{14}$$

where $B_{i,\,1}$ is called the absorption factor and by definition is the fraction of the total radiant energy emitted from surface i that is absorbed by surface 1. The three surfaces considered in this particular experiment are analyzed by the following equations:

$$(F_{1,\,1}r_1 - 1)B_{1,\,1} + F_{1,\,2}r_2 B_{2,\,1} + F_{1,\,3}r_3 B_{3,\,1} + F_{1,\,1}\epsilon_1 = 0 \tag{15}$$

$$F_{2,1}r_1B_{1,1} + (F_{2,2}r_2 - 1)B_{2,1} + F_{2,3}r_3B_{3,1} + F_{2,1}\epsilon_1 = 0 \tag{16}$$

$$F_{3,1}r_1B_{1,1} + F_{3,2}r_2B_{2,1} + (F_{3,3}r_3 - 1)B_{3,1} + F_{3,1}\epsilon_1 = 0 \tag{17}$$

This method of analysis (eqs. (15) to (17)) requires a knowledge of the geometry between the three surfaces, the average temperature of the surfaces, and the emissivity and reflectivity of the surfaces as given in reference 2.

The heat transferred by solid conduction through the vent tubes and instrumentation wiring can be expressed in the following manner:

$$\frac{d}{dx}\left(k\frac{dT}{dx}\right) = 0 \qquad \begin{cases} x = 0 \text{ at } T = T_1 \\ x = L \text{ at } T = T_2 \end{cases} \tag{18}$$

The thermal conductivity k is expressed as a function of the absolute temperature $k = k(T)$; substituting into equation (18) and integrating yield

$$k(T)\frac{dT}{dx} = C_1 = -\frac{q}{A}$$

$$\int_{T_1}^{T_2} k(T)dT = C_1\int_0^L dx = -\frac{q}{A}L$$

$$\frac{q}{A} = -\frac{1}{L}\int_{T_1}^{T_2} k(T)dT = k_m\frac{(T_1 - T_2)}{L}$$

where

$$k_m = \frac{1}{T_2 - T_1}\int_{T_1}^{T_2} k(T)dT$$

For the stainless steel tubing

$$k(T) = 0.0418T - 0.814\times10^{-4}T^2 + 6.25\times10^{-8}T^3 \qquad \frac{\text{Btu}}{(\text{hr})(\text{ft})(^{\circ}\text{R})}$$

For the wires a straight-line relation was assumed between two reference points:

$$k(T)_{Manganin} = 0.0203\ T + 2.200$$

$$k(T)_{copper} = 245.24 - 0.0405\ T$$

Heat transfer by gaseous conduction was negligible compared to the radiation transfer because of the very low vacuum (less than 0.001 μ) which existed during the test.

The heat stored in the contained hydrogen may be expressed by

$$\Delta Q_{st} = Wc_p\ \Delta T$$

REFERENCES

1. Otto, Edward W.: Static and Dynamic Behavior of the Liquid-Vapor Interface During Weightlessness. Preprint No. 17a, A. I. Ch. E., 1965.

2. Reynolds, William C.: Hydrodynamic Considerations for the Design of Systems for Very Low Gravity Environments. Rept. No. LG-1, Stanford Univ., Sept. 1961.

3. Benedikt, E. T.: Epihydrostatics of Liquids in Vertical Tanks. Rept. No. ASG-TM-61-48, Norair Div., Northrop Corp., June 1961.

4. Li, Ta: Hydrostatics in Various Gravitational Fields. J. Chem. Phys., vol. 36, no. 9, May 1, 1962, pp. 2369-2375.

5. Petrash, Donald A.; Zappa, Robert F.; and Otto, Edward W.: Experimental Study of the Effects of Weightlessness on the Configuration of Mercury and Alcohol in Spherical Tanks. NASA TN D-1197, 1962.

6. Petrash, Donald A.; Nussle, Ralph C.; and Otto, Edward W.: Effect of Contact Angle and Tank Geometry on the Configuration of the Liquid-Vapor Interface During Weightlessness. NASA TN D-2075, 1963.

7. Clodfelter, Robert G.: Fluid Mechanics and Tankage Design for Low-Gravity Environment. Rept. No. ASD-TDR-63-506, Air Force Systems Command, Wright-Patterson Air Force Base, Sept. 1963.

8. Petrash, Donald A.; Nelson, Thomas M.; and Otto, Edward W.: Effect of Surface Energy on the Liquid-Vapor Interface Configuration During Weightlessness. NASA TN D-1582, 1963.

9. Petrash, Donald A.; and Otto, Edward W.: Controlling the Liquid-Vapor Interface Under Weightlessness. AIAA J., vol. 2, no. 3, Mar. 1964, pp. 56-61.

10. Petrash, Donald A.; Nussle, Ralph C.; and Otto, Edward W.: Effect of the Acceleration Disturbances Encountered in the MA-7 Spacecraft on the Liquid-Vapor Interface in a Baffled Tank During Weightlessness. NASA TN D-1577, 1963.

11. Benedikt, E. T.: General Behavior of a Liquid in a Zero or Near Zero Gravity Environment. Rept. No. ASG-TM-60-9Z6, Norair Div., Northrop Corp., May 1960.

12. Masica, William J.; Petrash, Donald A.; and Otto, Edward W.: Hydrostatic Stability of the Liquid-Vapor Interface in a Gravitational Field. NASA TN D-2267, 1964.

13. Rohsenow, W. M.: A Method of Correlating Heat-Transfer Data for Surface Boiling of Liquids. Trans. ASME, vol. 74, no. 6, Aug. 1952, pp. 969-975.

14. Siegel, R.; and Usiskin, C. M.: A Photographic Study of Boiling in the Absence of Gravity. J. Heat Transfer (Trans. ASME), ser. C, vol. 81, no. 3, Aug. 1959, pp. 230-236.

15. Usiskin, C. M.; and Siegel, R.: An Experimental Study of Boiling in Reduced and Zero Gravity Fields. J. Heat Transfer (Trans. ASME), ser. C, vol. 83, no. 3, Aug. 1961, pp. 243-251; discussion, pp. 251-253.

16. Merte, Herman, Jr.; and Clark, J. A.: Pool Boiling in an Accelerating System. J. Heat Transfer (Trans. ASME), ser. C, vol. 83, no. 3, Aug. 1961, pp. 233-242.

17. Forster, H. K.; and Zuber, N.: Growth of a Vapor Bubble in a Superheated Liquid. J. Appl. Phys., vol. 25, no. 4, Apr. 1954, pp. 474-478.

18. Sherley, J. E.; and Merino, F.: Zero-G Program. NASA CR-51278, 1962.

19. Knoll, Richard H.; Smolak, George R.; and Nunamaker, Robert R.: Weightlessness Experiments with Liquid Hydrogen in Aerobee Sounding Rockets; Uniform Radiant Heat Addition - Flight 1. NASA TM X-484, 1962.

20. McArdle, Jack G.; Dillon, Richard C.; and Altmos, Donald A.: Weightlessness Experiments with Liquid Hydrogen in Aerobee Sounding Rockets; Uniform Radiant Heat Addition - Flight 2. NASA TM X-718, 1962.

21. Nunamaker, Robert R.; Corpas, Elias L.; and McArdle, Jack G.: Weightlessness Experiments with Liquid Hydrogen in Aerobee Sounding Rockets; Uniform Radiant Heat Addition - Flight 3. NASA TM X-872, 1963.

22. Regetz, John D., Jr.; Conroy, Martin J.; and Jackson, Robert G.: Weightlessness Experiments with Liquid Hydrogen in Aerobee Sounding Rockets; Nonuniform Radiant Heat Addition - Flight 4. NASA TM X-873, 1964.

23. Wallner, Lewis E.; and Nakanishi, Shigeo: A Study of Liquid Hydrogen in Zero Gravity. NASA TM X-723, 1963.

24. Abdalla, Kaleel L.; Flage, Richard A.; and Jackson, Robert G.: Zero-Gravity Performance of Ullage Control Surface with Liquid Hydrogen While Subjected to Unsymmetrical Radiant Heating. NASA TM X-1001, 1964.

25. Aydelott, John C.; Corpas, Elias L.; and Gruber, Robert P.: Comparison of Pressure Rise in a Hydrogen Dewar for Homogeneous, Normal-Gravity Quiescent, and Zero-Gravity Conditions - Flight 7. NASA TM X-1006, 1964.

26. Aydelott, John C.; Corpas, Elias L.; and Gruber, Robert P.: Comparison of Pressure Rise in a Hydrogen Dewar for Homogeneous, Normal-Gravity Quiescent, and Zero-Gravity Conditions - Flight 9. NASA TM X-1052, 1965.

27. Smalley, R. A.: Test Evaluation Report, Scientific Passenger Pod 18. Rept. No. GD/A-AAX64-002, General Dynamics/Astronautics, Apr. 8, 1964.

28. Roder, Hans M.; and Goodwin, Robert D.: Extended Tables of Provisional Thermodynamic Functions for Para Hydrogen (British Units), in Liquid, Fluid, and Gaseous States at Pressures to 5000 PSI, 36 to 180° R, and at Pressures to 1500 PSIA, 140 to 540° R. Rep. 7220, NBS, Jan. 3, 1962.

29. Gebhart, Benjamin: Heat Transfer. McGraw-Hill Book Co., Inc., 1961.

NASA-Langley, 1965 E-2875